

Evaluating Generatively Synthesized Diabetic Retinopathy Imagery

Cristina-Madalina Dragan  and Ruairi O'Reilly 
 Munster Technological University, Cork, Ireland
 cristina.madalina.dragan@gmail.com, ruairi.oreilly@mtu.ie

arXiv:2208.05593v1 [eess.IV] 10 Aug 2022

Abstract—Publicly available data for the training of diabetic retinopathy classifiers is unbalanced. Generative adversarial networks can successfully synthesize retinal fundus imagery. In order for synthetic imagery to be of benefit, images need to be of high quality and diverse. Presently, several evaluation metrics are used to evaluate the quality and diversity of imagery synthesized from generative adversarial networks. This work contributes, the first of its kind, empirical assessment for the suitability of evaluation metrics used in the literature for the evaluation of generative adversarial networks for generating retinal fundus images in the context of diabetic retinopathy. Fréchet Inception Distance, Peak Signal-to-Noise Ratio and Cosine Distance’s capacity to assess the quality and diversity of synthetic proliferative diabetic retinopathy imagery is investigated. A quantitative analysis is performed to enable an improved methodology for selecting the synthetic imagery to be used for augmenting a classifier’s training dataset. Results indicate that Fréchet Inception Distance is suitable for evaluating the diversity of synthetic imagery, and for identifying if the imagery has features corresponding to its class label. Peak Signal-to-Noise Ratio is suitable for indicating if the synthetic imagery has valid diabetic retinopathy lesions and if its features correspond to its class label. These results demonstrate the importance of performing such empirical evaluation, especially in the context of biomedical domains where utilisation in applied setting is intended.

Index Terms—Image synthesis, Data augmentation, Fréchet Inception Distance, Peak signal-to-noise ratio, Cosine Distance, Convolutional neural networks, Generative adversarial networks, Deep learning.

1 INTRODUCTION

Diabetic retinopathy (DR) is a complication caused by high blood sugars level over a prolonged period that is estimated to affect 415 million people globally [1] and can lead to blindness if it is not treated. Diagnosis is made based on the analysis of retinal fundus imagery, where lesions specific to DR are identified. The severity of DR is evaluated using the international severity grading scale (ISGR), which has four stages [2]: Mild Non-Proliferative DR (Mild NPDR), Moderate NPDR, Severe NPDR and Proliferative DR (PDR)

(see Figure 1). The increasing prevalence of the disease and the lack of medical personnel capable of diagnosing it highlights the need for computer aided diagnostics to assist healthcare professionals [3], [4], [5].

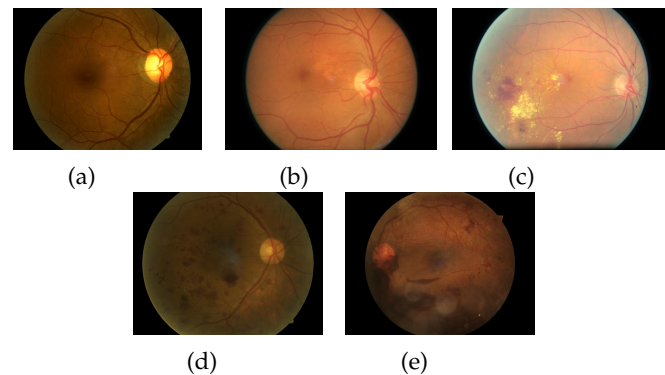


Fig. 1: Retinal fundus images with different stages of DR: (a) No DR (b) Mild NPDR (c) Moderate NPDR (d) Severe NPDR (e) PDR

Publicly available retinal fundus image datasets are imbalanced, containing significantly more images without DR than images depicting different DR stages. The availability of images decreases as the severity of DR increases, with severe NPDR and PDR accounting for a total of 4% of the available images (see Table 1). One solution to address the issue of data imbalance is to augment training data with synthetic imagery belonging to the underrepresented classes.

Synthetic retinal fundus imagery can be obtained with generative models capable of generating synthetic imagery. Generative Adversarial Networks (GANs) are generative models consisting of two neural networks, a generator and a discriminator. The generator aims to produce realistic synthetic images, and the discriminator’s aim is to distinguish between real and synthetic images.

Two critical criteria for evaluating synthetically generated images are the quality of the images, indicating how representative they are of that class, and the diversity of the images, indicating how broad and uniform the coverage of their feature distribution is. The quality of synthetic imagery is characterised by an alignment of its feature distribution

Dataset	No. Img	No DR	Mild NPDR	Mod. NPDR	Sev. NPDR	PDR
Kaggle [6]	88702	65343	6205	13153	2087	1914
APTOS [7]	3662	1805	370	999	193	295
Messidor-2 [8], [9]	1744	1017	270	347	75	35
Messidor* [8]	1200	546	153	247	254	-
IDRID [10]	516	168	25	168	93	62
DR2 [11]	435	98	337	-	-	-
1000	144	38	18	49	39	-
Fundus [12]						
STARE [13]	113	41	51	21	-	-
HRFID [14]	30	15	15	-	-	-
Total*	95346	68525	7291	14737	2487	2306
As %		.72	.08	.15	.02	.02

TABLE 1: Publicly available datasets containing retinal fundus images at different stages of DR. * Messidor excluded from total as 1058 images overlap with the Messidor-2 dataset

with the class label [15], [16], [17] and by having a low level of noise, blurriness and distortions [18]. The diversity of synthetic images is characterised by the level of similarity to each other [19].

Suppose the training dataset is augmented with low-quality synthetic images. In that case, the classifier will not learn the features representative of different classes, and the classification performance will be affected. Suppose the training dataset is augmented with images that lack diversity. In that case, the dataset provides limited coverage of the target domain resulting in a higher likelihood that the classifier will incorrectly classify images containing feature distributions that belong to the less represented areas. When synthetic images are used for training a classifier, it is essential that they are of high quality and that the features representative of a class are sufficiently diverse.

Quality of synthetic imagery represents the level of similarity to the real imagery; diversity represents the level of dissimilarity between the synthetic imagery. There are several metrics for evaluating the similarity between images [20], [21], [22]. Some are manual, time-consuming and subjective [21], as they depend on the domain knowledge of the individual evaluating the images. Others are calculated quantitatively. In this work, three quantitative evaluation metrics are considered: Cosine Distance (CD), Fréchet Inception Distance (FID) and Peak Signal-to-Noise Ratio (PSNR).

As PDR is the most severe stage of DR with the lowest quantity of publicly available images, this work narrows its focus to the generation of synthetic PDR imagery. In the context of PDR, a high-quality synthetic image depicts the presence of valid lesions specific to PDR, and a high level of diversity is indicated by the presence of lesions of different sizes, shapes and locations.

To date, the quality and diversity of synthetic retinal fundus imagery with DR have been evaluated using FID and CD. However, no assessment as to the suitability of the metrics has been performed to best of the authors’ knowledge. This work contributes: (i) a critical analysis of quantitative evaluation metrics’ capacity to identify if imagery contains

Ref	Year	Model	Dataset	Acc.	Mac. F1
[27]	2020	CNN (Feat. extr.), Dec. tree (J48)	Kaggle IDRI	99.99	0.999*
[28]	2019	Inception V4	Private	99.03	0.987*
[29]	2019	Siamese CNN	Kaggle	88.4	0.678*
[4]	2017	CNN/Denoising	Kaggle	84.25*	0.603*
[30]	2019	Ensemble/Transfer Learning	Kaggle	85	0.566*
[31]	2018	Deep CNN, special class coding technique	Kaggle	80.8	0.532
[32]	2016	Deep CNN	Kaggle	50.8	0.482*
[3]	2019	CNN	Kaggle	73.76*	0.335*
[5]	2019	Deep CNN, selective data sampling	Kaggle	74	-
				87.2	-

TABLE 2: CNN based classification of DR stages based on the ISGR. * derived performance from confusion matrix

features corresponding to its class label, (ii) an investigation of GAN’s capacity to generate synthetic PDR images and (iii) an evaluation of the relationship between diversity and quality of the synthetic imagery as indicated by FID, PSNR and CD, and classification performance.

It is envisaged that knowing which evaluation metrics are suitable for evaluating the quality and diversity of synthetic retinal fundus imagery enables a better selection of the synthetic imagery that will be used to augment the training dataset of a classifier.

2 RELATED WORK

Several state-of-the-art works for automatically classifying DR via retinal fundus imagery that use Convolutional Neural Networks (CNNs) are denoted in Table 2. In order for CNNs to generalise across DR stages whilst achieving a performant classification accuracy, they need to be trained on a large and balanced dataset [23], [24].

In detailing the CNNs in Table 2 macro-averaged F1 score (mac. F1) was used to compare their performance, as all classes are treated equally [25]. This is particularly important due to the data imbalance and the minority class (PDR) being the most severe stage of DR. The macro-averaged F1 score was calculated based on the mean of the F1 scores for every class [26].

Data augmentation is one approach to address data imbalance when training a CNN. It consists of adding synthetic or modified versions of the original images from the underrepresented classes to the dataset [3], [27], [33], [34]. Modified versions of the original images can be obtained with rotation, flipping or random cropping techniques. The limitation of these techniques is that the diversity of the resulting dataset is limited [15], [35]. An alternate technique is the generation of synthetic imagery using GANs to augment the training data.

2.1 Generative approaches to addressing data imbalance for DR

Medical datasets are often imbalanced [36], [37], as such, there has been extensive work in generating synthetic medical imagery in the scientific community (see Table 3).

Quality and diversity of synthetic medical imagery is evaluated manually by physicians and quantitatively with evaluation metrics such as Structural Similarity Index Measure (SSIM), PSNR, FID, etc. It can be seen in Table 3 that there is no accepted consensus for evaluating the quality and diversity of generated imagery. Also, significantly more emphasis has been placed on evaluating the quality of the generated imagery than on evaluating the diversity. This is because it is challenging to avoid mode collapse when training GANs.

In this work, these perspectives have acted as motivating factors, for enabling a more transparent assessment of a GANs capacity to generate suitably diversified retinal fundus images with PDR.

To demonstrate the benefits of generating synthetic imagery, in several works the training dataset is augmented with the synthetic images and classification performance is calculated with evaluation metrics like accuracy, sensitivity, precision, kappa and specificity.

In [15] a conditional GAN (CGAN) is used to generate retinal fundus images for each DR stage. Quality is evaluated using three methods: manual evaluation, FID and Sliced Wasserstein distance (SWD). Five hundred real and five hundred synthetic images are mixed, and two experiments are undertaken. Three ophthalmologists labelled each image as real or synthetic and assigned a severity level of DR. FID and SWD were calculated between the real and synthetic images.

In [43] a deep convolutional GAN (DCGAN) is used to generate retinal fundus images of PDR. Quality and diversity are evaluated using average CD. The synthetic images are added to the training dataset. The InceptionV3 model pre-trained on the ImageNet database extracts features from the images with PDR from the augmented dataset. The CDs between the extracted features are calculated and their average is compared to the average of the CDs between the features extracted only from the real images with PDR.

In [35] a StyleGAN is used to generate retinal fundus images with referable DR (a combination of moderate NPDR, severe NPDR and PDR) and vision-threatening DR (PDR). It is not specified how the GAN is evaluated.

A limiting factor of existing works is that the method of selecting the synthetic images used for data augmentation is not specified. In the works where the quality and diversity of the synthetic images are evaluated, it is not assessed whether the metrics used are suitable to evaluate the quality and diversity of the generated imagery.

PSNR [49] evaluates the quality of reconstructing images or expanding their dimensions. PSNR has been used for evaluating the quality of synthetic brain PET imagery and synthetic retinal fundus images, healthy and with glaucoma. The rationale for including it is based on pixel intensities, unlike FID and CD, which are based on extracted features, and therefore depend on the feature extraction method.

3 METHODOLOGY

The following sections describe the dataset used and the methodology for: (i) analysing evaluation metrics' capacity to identify if an image contains features corresponding to its class label (ii) the generation of synthetic PDR imagery and (iii) correlating diversity, quality and classification performance.

3.1 Retinal fundus imagery

Publicly available retinal fundus imagery is imbalanced and increasingly limited as the severity of DR increases. As denoted in Table 1, PDR is the minority class associated with DR. It was decided to narrow the focus of synthetic data generation to retinal fundus imagery with PDR.

In this work the Kaggle dataset [6] is used, which is the largest publicly available dataset containing retinal fundus images from patients with different DR stages. Table 4 denotes the number of images per stage of DR available in the training and test dataset.

3.2 Evaluation metrics' capacity to identify if imagery contains features corresponding to its class label

A metric can identify if an image contains features corresponding to its class label if for any image X belonging to class C , the metric indicates a higher similarity between X and other images of class C than between X and images belonging to other classes.

To assess the evaluation metrics' (FID, PSNR and CD) capacity to identify if retinal fundus imagery contains features corresponding to its class label, 300 images of each DR stage were randomly selected from the training and test datasets and resized to resolution 128x128. The similarity between images with different severity levels of DR was calculated using the three evaluation metrics. This process was performed separately for the training and test datasets.

3.2.1 Evaluation metrics

The equations for FID, PSNR and CD are denoted in equations (1), (3) and (4), respectively.

$$PSNR(img1, img2) = 10 \cdot \log_{10} \cdot \frac{255}{MSE(img1, img2)} \quad (1)$$

$$MSE(img1, img2) = \frac{1}{no. \ pix} \cdot \sum_{n=1}^{no. \ pix} (pix \ n_{img1} - pix \ n_{img2})^2 \quad (2)$$

$$CD(f1, f2) = 1 - \frac{\vec{f1} \cdot \vec{f2}}{\|\vec{f1}\| \times \|\vec{f2}\|} \quad (3)$$

$$FID(x, y) = \|m1 - m2\|^2 + Tr(C1 + C2 - 2 \cdot \sqrt{C1 \times C2}) \quad (4)$$

$f1$ and $f2$: feature vectors extracted from 2 images. In this work the features are extracted from an InceptionV3 model pre-trained on the ImageNet dataset. $m1$ and $m2$: vectors containing the mean of every feature, from sets of images x and y , respectively. Tr : trace, representing the sum of the elements from the main diagonal of a matrix. $C1$, $C2$: covariance matrices for the feature vectors from the sets of images x and y , respectively.

Ref	Year	GAN	Classifier	Classif. gain	Quality eval.	Diversity eval.
[38]	2019	DCGAN	CNN (new arch.)	Sens: 0.12 Spec: 0.12	N/A	N/A
[39]	2019	Cond. PGGAN	YOLOv3 CNN [40]	Sens: 0.1	Visual Turing Test	T-SNE
[41]	2020	DCGAN	CNN (arch. unspec.)	Acc: 0.1	PSNR, SSIM, 2D histogram	N/A
[15]	2020	CGAN	VGG-16, ResNet-50, I-v3, AFN, Zoom-in	Acc: 0.01 Kappa: 0.09	FID, SWD, evaluation by ophthalmologists	N/A
[42]	2018	DCGAN, AC-GAN	CNN (new arch.)	Sens: 0.07 Spec: 0.04	Assessment by radiologists	N/A
[43]	2020	DCGAN	CNN (new arch.)	Prec: 0.04 Rec: 0.05 F1: 0.06	CD	CD
[44]	2019	PGGAN, SimGAN	ResNet-50	Acc: 0.03 Sens: 0.04 Spec: 0.02	Visual Turing Test, T-SNE	T-SNE
[45]	2019	ProGAN	ResNet-50	N/A	Assess. by retinal specialists	N/A
[46]	2019	DCGAN, SS-DCGAN	SS-DCGAN	N/A	LSE, T-SNE, AVP, MSE	AVP, MSE
[47]	2020	CGAN	N/A	N/A	N/A	N/A
[16]	2018	CGAN	N/A	N/A	ISC score, visual eval.	N/A
[48]	2020	SynSig GAN	N/A	N/A	RMSE, PRD, MAE, FD, PCC	N/A
[17]	2019	Pix2pix, Cycle-GAN	N/A	N/A	SSIM, PSNR, visual eval.	N/A
[35]	2020	StyleGAN	ResNet-50	N/A	N/A	N/A

TABLE 3: Generation of biomedical imagery utilising GANs. Classification performance gain is noted where generated images were used in training a classifier (Accuracy: Acc, average proportion of pixels belonging to the vessel and optic disc: AVP, F1 score: F1, Image Structure Clustering Score: ISC score, Inception-v3: I-v3, Kappa score: Kappa, Latent space exploration: LSE, Mean Absolute Error: MAE, Mean Squared Error between 2D histograms: MSE, Pearson’s Correlation Coefficient: PCC, Percent Root Mean Square Difference: PRD, Precision: Prec, Recall: Rec, Root Mean Square Error: RMSE, Sensitivity: Sens, Specificity: Spec, t-Distributed Stochastic Neighbor Embedding: T-SNE).

	No DR	Mild NDPR	Mod. NDPR	Severe NDPR	PDR
Train	25810	2443	5292	873	708
Test	39533	3762	7861	1214	1206

TABLE 4: Images per DR stage in the training and test datasets [6].

3.2.2 Normalising results

The returned values are normalised to a 0 to 1 range via equations (5), (6) and (7). A high similarity between two sets of images is indicated by high values of the normalised evaluation metrics.

$$\text{Normalised PSNR} = \frac{\text{PSNR} - \min \text{PSNR}}{\max \text{PSNR} - \min \text{PSNR}} \quad (5)$$

$$\text{Normalised FID} = 1 - \frac{\text{FID} - \min \text{FID}}{\max \text{FID} - \min \text{FID}} \quad (6)$$

$$\text{Normalised CD} = 1 - \frac{\text{CD} - \min \text{CD}}{\max \text{CD} - \min \text{CD}} \quad (7)$$

Normalisation of the results obtained for each evaluation metric in each experiment is done independently. The normalised results obtained in different experiments or for different evaluation metrics are therefore not comparable.

3.3 Generating synthetic PDR imagery

Synthetic images containing PDR should depict valid representations of the retinal fundus with features that are characteristic of PDR. Moreover, generated images should depict the lesions specific to PDR in diverse areas of the retina. The challenge lies in quantitatively evaluating the quality and diversity of synthetic imagery generated.

In order to assess the evaluation metrics, a Deep Convolutional GAN (DCGAN) [50] is trained to generate synthetic retinal fundus imagery with PDR. 125 sets of synthetic images are generated throughout the DCGAN training. The sets of images containing features corresponding to PDR are selected. The quality and diversity of each selected set of images are evaluated using FID, PSNR and CD. The diversity of each set of synthetic imagery is compared to the diversity of the real images of PDR. The returned values are normalised to a 0 to 1 range via equations (5), (6) and (7). Quality is indicated by high values of the normalised evaluation metrics, and diversity is indicated by low values of the normalised evaluation metrics.

The DCGAN is based on an implementation specified in [43], with the addition of dropout to all layers. The architecture is depicted in Figure 2a. The DCGAN is trained for 125 epochs with batch size 4. An SGD optimiser is used to train the discriminator, and an Adam optimiser is used to train the generator. The learning rate is 0.0001 for both the discriminator and the generator. The DCGAN generates 708 images after every epoch of training.

3.4 Correlating quality, diversity and classification performance

A classifier is trained to classify DR stages. Each of the selected sets of synthetic imagery is added to the training dataset for the classifier and the classification performance is calculated.

As classification performance is higher when the training images are of high quality, a metric is considered suitable for evaluating the quality of synthetic imagery if a high quality indicated by that metric aligns with a high classification performance. Similarly, as classification performance is higher when the training images are diverse, a metric is considered suitable for evaluating the diversity of synthetic imagery if a high diversity indicated by that metric aligns with a high classification performance.

The quality and diversity scores are analysed using each evaluation metric and correlated against the classification performance. The intent is to assess the metrics' suitability for evaluating the quality and diversity of synthetic imagery.

3.4.1 Evaluation of classification performance

A state-of-the-art classifier for DR [27] is reimplemented (see Figure 2b). A CNN is used for feature extraction and a Random Forest model for classification. 32 features are extracted from the second Dense layer of the CNN. Multi-class classification is performed to identify the severity of DR aligned with the ISGR stages.

The training dataset is highly imbalanced; [27] does not state what method is used in training to avoid obtaining a biased model that assigns the majority class to most of the instances. In this work, class weights are used to address this bias. Class weight values are selected using equation 8 [51], corresponding to the "balanced" value of the *class_weight* parameter from the scikit-learn library [52].

$$\text{Class weight class } x = \frac{\text{Total num. of images}}{\text{Num. classes} \times \text{Num. img cls } x} \quad (8)$$

Classification performance is evaluated with the Area Under the Curve (AUC). AUC is chosen over F1 score as it measures how accurate the border between the classes is identified by the classifier. The one-versus-rest (OVR) approach [53] is used for calculating AUC, with equation 9.

$$\text{AUC}_{\text{OVR}} = \frac{1}{c} \sum_{i=0}^{c-1} \text{AUC}(C_i, C_i^C) \quad (9)$$

c : number of classes, C_i : images with class label i , C_i^C : the complement set of C_i

3.4.2 Correlating quality and diversity of synthetic imagery with classification performance

AUC is segregated on intervals (0.51-0.6, 0.61-0.7, 0.71-0.8, 0.81-0.9 and 0.91-1). The distribution of quality and diversity of the synthetic images used for augmentation is evaluated with normalised FID, CD and PSNR. This is done to assess if the evaluation metrics correlate with the classification performance and, therefore, are good indicators of the quality and diversity of synthetic imagery. In this experiment,

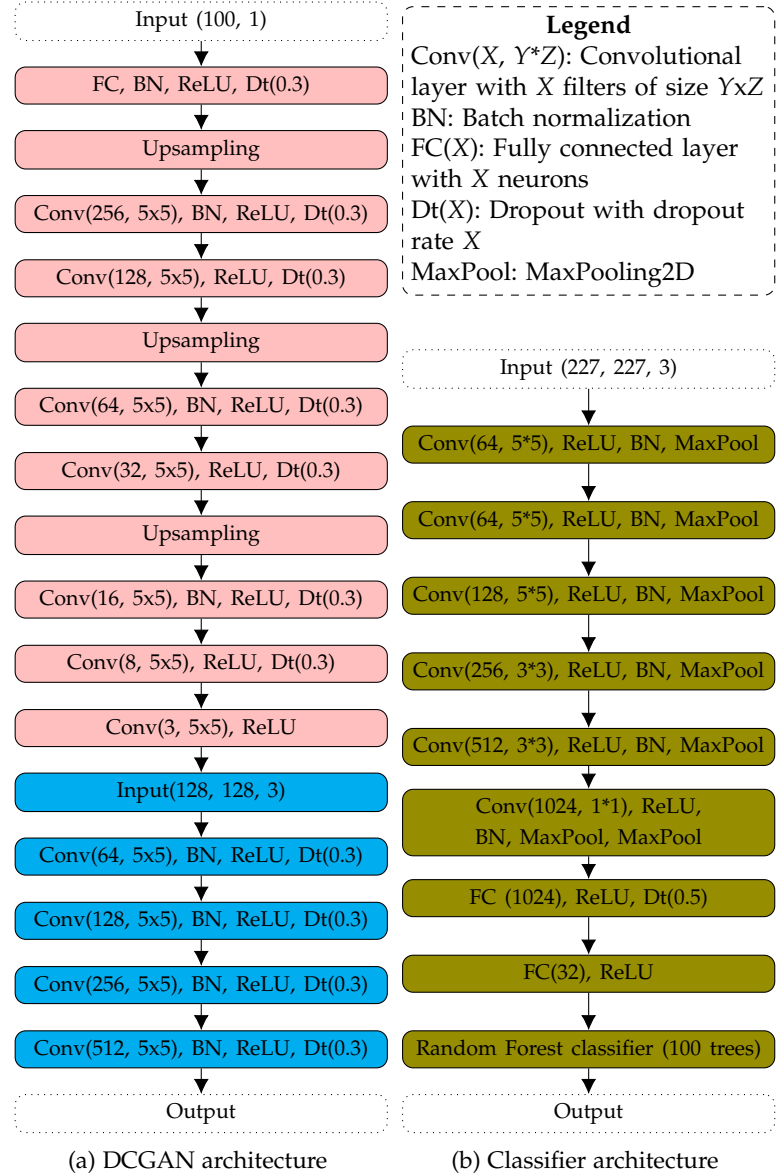


Fig. 2: Architectures of DCGAN (left) and classifier (right)

normalisation is only performed with synthetic images as the quality and diversity of the real images are irrelevant.

4 RESULTS AND DISCUSSION

The results are aligned with the following research aims: 4.1. Critical analysis of quantitative evaluation metrics to identify if an image contains features corresponding to its class label, 4.2. Investigation of a DCGAN's capacity to generate synthetic PDR images and 4.3. Evaluation of the relationship between diversity and quality of the synthetic imagery and classification performance.

4.1 Critical analysis of quantitative evaluation metrics

The similarity between retinal fundus images with different stages of DR measured with FID, CD and PSNR is denoted in Table 5. Results indicate that on a per DR stage basis, the FID and PSNR indicate a higher similarity between images with the same class label than between images with different

Eval. metric, dataset	Class	No DR	Mild NPDR	Mod. NPDR	Sev. NPDR	PDR
PSNR, Training data	No DR	1	0.029	0.037	0.047	0.013
	Mild NPDR	0.029	0.212	0.016	0.032	0
	Mod. NPDR	0.037	0.016	0.21	0.032	0.002
	Sev. NPDR	0.047	0.032	0.032	0.25	0.017
PSNR, Test data	No DR	0.998	0.137	0.394	0.384	0.204
	Mild NPDR	0.137	0.548	0.139	0.139	0
	Mod. NPDR	0.394	0.139	1	0.394	0.206
	Sev. NPDR	0.384	0.139	0.394	0.998	0.219
FID, Training data	No DR	>.999	0.019	0.028	0.041	0
	Mild NPDR	0.019	1	0.82	0.797	0.688
	Mod. NPDR	0.028	0.82	>.999	0.799	0.736
	Sev. NPDR	0.041	0.797	0.799	>.999	0.709
FID, Test data	No DR	1	0.871	0.126	0.204	0.019
	Mild NPDR	0.871	>.999	0.148	0.203	0
	Mod. NPDR	0.126	0.148	>.999	0.152	0.126
	Sev. NPDR	0.204	0.203	0.152	>.999	0.132
CD, Training data	No DR	0.394	0	0.091	0.152	0.031
	Mild NPDR	0	0.697	0.758	0.849	0.697
	Mod. NPDR	0.091	0.758	0.879	0.94	0.788
	Sev. NPDR	0.152	0.849	0.94	1	0.849
CD, Test data	No DR	0.237	0.064	0.297	0.073	0.457
	Mild NPDR	0.064	0.214	0.191	0	0.398
	Mod. NPDR	0.297	0.191	0.516	0.204	0.625
	Sev. NPDR	0.073	0	0.204	0.058	0.323
	PDR	0.457	0.398	0.625	0.323	1

TABLE 5: Similarity between sampled retinal fundus images with different stages of DR measured via FID, CD and PSNR

class labels. Therefore, FID and PSNR are suitable metrics for evaluating if the synthetic imagery is representative of its class label. This enables a selection of suitable synthetic imagery for data augmentation when training a classifier. As FID makes a clear distinction between images belonging to the same class and images belonging to different classes, in this work FID is used to assess if the synthetic images belong to the correct class label. It was found that all sets of synthetic images belong to the correct class label.

PSNR and FID are suitable metrics for evaluating if the synthetic imagery is representative of its class label because of how they are calculated. PSNR is calculated based on pixel intensities. Lesions specific to DR have specific pixel intensities, and the number of pixels with these intensity levels is a good indicator of the severity level of DR. Whilst ImageNet does not contain retinal fundus images with DR, it contains a large number of labels representing a diverse set of objects. Features extracted from retinal fundus images are highly representative of the DR stage. CD is not a suitable metric for evaluating if the synthetic imagery is

representative of its class because it is calculated based on the angle between the extracted features. If the angle between two feature vectors is zero, they are not necessarily identical.

An interesting observation from Table 5 is the significant difference in the distribution of values derived from the training and test datasets. This indicates that the datasets have a different feature distribution. It is important to identify this as:

i) If a classifier is trained on the training dataset, the feature distribution could significantly impact its performance from an evaluation performed on the test data. Although not stated in prior literature, this is a probable rationale for model evaluation being solely performed on images from the Kaggle training dataset in: [30], [3], [29], [4] and [27].

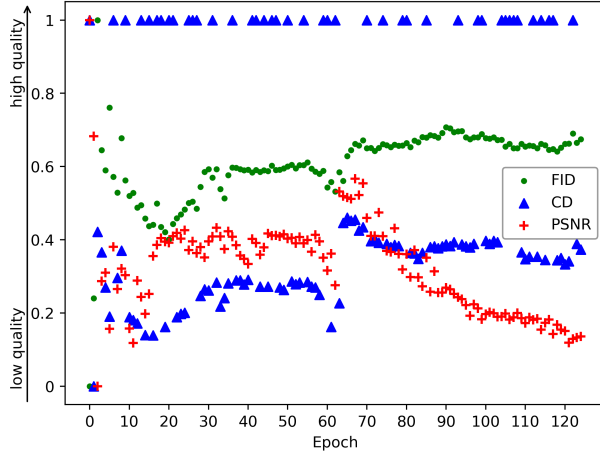
ii) When relying on evaluation metrics to assess the quality of synthetic imagery, the synthetic imagery generated must be compared to real class instances to assess if it contains the features representative of its class label. As the train and test datasets have different feature distributions, the synthetic images should be compared to class instances from the dataset used for training the GAN.

4.2 Generating synthetic PDR imagery

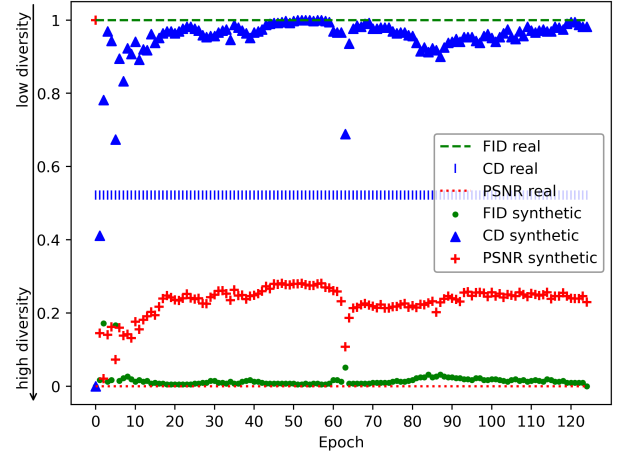
The quality of each set of synthetic images derived via the evaluation metrics is depicted in Figure 3a. While FID indicates that the imagery generated in the last epochs of training has higher quality than the imagery generated in the early epochs, PSNR indicates the opposite. Similarly, between epochs 62 and 65 FID indicates a drop in the quality, while PSNR indicates the opposite. CD oscillates throughout the training, indicating that there is a big difference in quality between images generated in consecutive epochs. There is no consensus between the three evaluation metrics on which sets of images have high quality.

The diversity of each set of synthetic images, and the diversity of the real images with PDR are denoted in Figure 3b. While PSNR indicates that the real images have a higher diversity than the synthetic ones, FID indicates the opposite. CD indicates that most sets of synthetic images have a lower diversity than the real images. CD and PSNR indicate that the images generated at the beginning of the training have a higher diversity than the images generated in the later epochs, while FID indicates the opposite. There is no agreement between the metrics on which sets of images are most diverse.

The reason why PSNR indicates that real images are more diverse than synthetic images is because the synthetic images do not capture a wide variety of light conditions, and their pixels are therefore more similar to each other. CD indicates that real imagery is more diverse than most sets of synthetic imagery because the features extracted from real imagery are less dependent on each other. Given feature vectors $f1$ and $f2$, containing features a and b , if $a1$ is the value of feature a in $f1$, $a2$ is the value of a in $f2$, $b1$ is the value of b in $f1$, $b2$ is the value of b in $f2$, if $\frac{a1}{b1} = \frac{a2}{b2}$, then the angle between them is zero, and CD indicates perfect similarity. FID indicates that the features from the synthetic imagery are spread over a larger area.



(a) Quality



(b) Diversity

Fig. 3: Quality and diversity of the synthetic retinal fundus imagery with PDR generated while training the DCGAN.

Classifier	k-fold	Class weights	No DR	Mi. DR	Mod. DR	Sev. DR	PDR
Orig. [27]	n/a	n/a	0.999	0.999	1	0.974	0.981
α	5 fold	yes	0.753	0.214	0.434	0.607	0.774

TABLE 6: Classifiers' F1 scores.

4.3 Correlating quality, diversity and classification performance

Table 6 denotes the F1 scores obtained when the training was performed only on real imagery, in this work and in [27]. In [27] the value of k from k -fold validation and the method of addressing class imbalance are not specified. These two implementation details are probably different than in this work, and they are therefore the reason why the classification performance obtained in this work (α) is lower than in [27].

The AUC obtained when the training dataset was augmented with each set of synthetic images generated by the DCGAN can be seen in Figure 4. The classification performance when the training dataset is augmented oscillates, but it is higher when augmentation is done with images generated in the early epochs of the DCGAN training. This indicates that the synthetic images generated in the early epochs of the DCGAN training have higher quality and diversity.

Figure 4 denotes that when training is performed only on the real images AUC is 0.736, and when training is performed on augmented datasets the AUC has values between 0.6 and 1. It can be seen that augmenting the dataset with synthetic imagery can increase the classification performance significantly, if the images used for augmentation are of high quality and diversity. At the same time, augmenting the dataset with synthetic images can reduce the classification performance, if the images used for augmentation have low quality and diversity. This emphasizes the importance of using suitable images for data augmentation. It is also

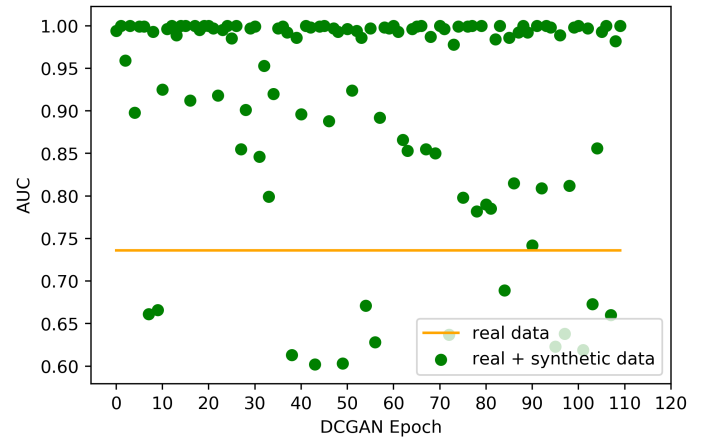


Fig. 4: The classification performance achieved when the classifier was trained on the original training dataset, containing real images, and on the training dataset augmented with 708 synthetic images with PDR generated in different epochs of the DCGAN training.

denoted in Figure 4 that data augmentation increased the AUC significantly more than it decreased it. This indicates that data augmentation with synthetic imagery is a promising solution for improving classification performance.

The distribution of quality of the synthetic images used for augmentation when the AUC obtained was in each interval is depicted in Figure 5. PSNR is generally higher when the AUC is high. PSNR is therefore suitable for evaluating the quality of synthetic imagery. This is because PSNR is calculated based on the pixel intensities, which are indicative of the DR lesions.

An interesting aspect depicted in Figure 5 is that even though there are significantly more AUC values in interval 0.91-1 than in the other intervals, the distribution of PSNR values in this interval is not wider than the distribution in the other intervals. This indicates that PSNR is consistent

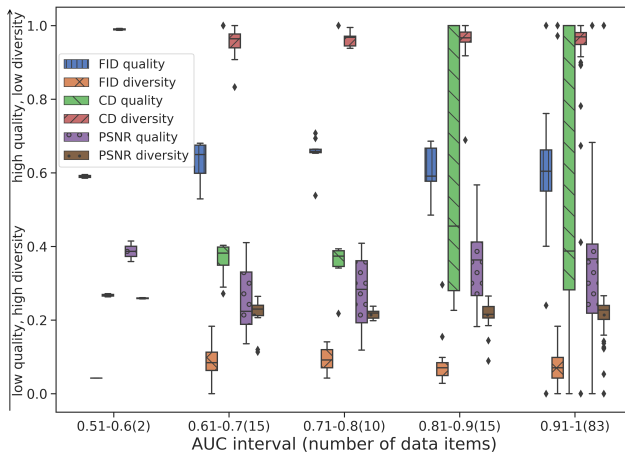


Fig. 5: Distribution of the quality and diversity of the sets of synthetic images used for augmentation, where the sets are grouped by the AUC achieved by the classifier trained on the augmented datasets.

and accurate in evaluating the quality of synthetic imagery.

The distribution of diversity of the synthetic images used for augmentation when the AUC obtained was in each interval is depicted in Figure 5. There is no clear correlation between the classification performance and the diversity as measured with PSNR, FID and CD, but FID and PSNR are generally lower when the AUC is high; they are therefore suitable for evaluating the diversity of synthetic imagery with DR.

FID is suitable for evaluating the diversity because the more diverse the images are, the more diverse the features extracted with the pre-trained InceptionV3 model are. It is not important if the features depend on each other, but rather how large their distribution is. CD is therefore not suitable for evaluating the diversity.

PSNR is suitable for evaluating the diversity because it is calculated based on the pixel intensities, which are good indicators of the DR lesions and light conditions. However, only the diversity of relevant pixels is relevant to the classifier. The relevant pixels are the pixels containing DR lesions. PSNR is therefore less suitable than FID for evaluating the diversity of synthetic imagery.

5 CONCLUSION

This work contributes an empirical interpretation of the selection process of synthetic retinal fundus imagery for data augmentation. The process has two stages, the first being the selection of the synthetic imagery containing features corresponding to its class label using FID or PSNR, and the second being the selection of the imagery where the lesions are valid and diverse, using PSNR and FID, respectively. There can be a trade-off between having valid and diverse lesions, but these criteria are not mutually exclusive.

The results demonstrate the importance of using an empirical approach for selecting the evaluation metrics for generative adversarial networks, especially in the context of

biomedical domains where utilisation in applied setting is intended.

REFERENCES

- [1] D. Cavan *et al.*, "The diabetic retinopathy barometer study: Global perspectives on access to and experiences of diabetic retinopathy screening and treatment," *Diabetes Res. and Clin. Pract.*, vol. 129, pp. 16–24, 2017.
- [2] C. Wilkinson *et al.*, "Proposed international clinical diabetic retinopathy and diabetic macular edema disease severity scales," *Ophthalmology*, vol. 110, no. 9, pp. 1677–1682, 2003.
- [3] M. Arora and M. Pandey, "Deep neural network for diabetic retinopathy detection," in *2019 Int. Conf. Mach. Learn., Big Data, Cloud and Parallel Comput. (COMITCon)*, pp. 189–193.
- [4] R. Ghosh, K. Ghosh, and S. Maitra, "Automatic detection and classification of diabetic retinopathy stages using cnn," in *2017 4th Int. Conf. Signal Process. and Integr. Netw. (SPIN)*, pp. 550–554.
- [5] J. Ni, Q. Chen, C. Liu, H. Wang, Y. Cao, and B. Liu, "An effective cnn approach for diabetic retinopathy stage classification with dual inputs and selective data sampling," in *2019 18th IEEE Int. Conf. Mach. Learn. And Appl. (ICMLA)*, pp. 1578–1584.
- [6] J. Cuadros and G. Bresnick, "Eyepacs: An adaptable telemedicine system for diabetic retinopathy screening," *J. of Diabetes Sci. and Technol.*, vol. 3, no. 3, pp. 509–516, 2009.
- [7] "APTOS 2019 Blindness Detection | Kaggle." [kaggle.com. https://www.kaggle.com/c/aptos2019-blindness-detection](https://www.kaggle.com/c/aptos2019-blindness-detection) (accessed Mar . 03, 2022).
- [8] E. Decencière *et al.*, "Feedback on a publicly distributed image database: The messidor database," *Image Anal. & Stereology*, vol. 33, no. 3, pp. 231–234, 2014.
- [9] M. D. Abràmoff *et al.*, "Automated Analysis of Retinal Images for Detection of Referable Diabetic Retinopathy," *JAMA Ophthalmology*, vol. 131, pp. 351–357, Mar. 2013.
- [10] P. Porwal *et al.*, "Indian diabetic retinopathy image dataset (idrid)," 2018. Distributed by IEEE Dataport. <https://dx.doi.org/10.21227/H25W98>.
- [11] R. Pires, H. F. Jelinek, J. Wainer, E. Valle, and A. Rocha, "Advancing Bag-of-Visual-Words Representations for Lesion Classification in Retinal Images," *PloS one*, vol. 9, no. 6, 2014.
- [12] L.-P. Cen *et al.*, "Automatic detection of 39 fundus diseases and conditions in retinal photographs using deep neural networks," *Nature communications*, vol. 12, no. 1, pp. 1–13, 2021.
- [13] A. Hoover, V. Kouznetsova, and M. Goldbaum, "Locating blood vessels in retinal images by piecewise threshold probing of a matched filter response," *IEEE Trans. on Med. Imag.*, vol. 19, no. 3, pp. 203–210, 2000.
- [14] J. Odstrcilik *et al.*, "Retinal vessel segmentation by improved matched filtering: evaluation on a new high-resolution fundus image database," *IET Image Process.*, vol. 7, pp. 373–383, Jun. 2013.
- [15] Y. Zhou, B. Wang, X. He, S. Cui, and L. Shao, "Dr-gan: Conditional generative adversarial network for fine-grained lesion synthesis on diabetic retinopathy images," *IEEE J. of Biomed. and Health Inform.*, 2020.
- [16] P. Costa *et al.*, "End-to-end adversarial retinal image synthesis," *IEEE Trans. on Med. Imag.*, vol. 37, no. 3, pp. 781–791, 2018.
- [17] Z. Yu, Q. Xiang, J. Meng, C. Kou, Q. Ren, and Y. Lu, "Retinal image synthesis from multiple-landmarks input with generative adversarial networks," *BioMed. Eng. OnLine*, vol. 18, May 2019.
- [18] K.-H. Thung and P. Raveendran, "A survey of image quality measures," in *2009 Int. Conf. for Knowl. Tech. Postgraduates (TECHPOS)*, pp. 1–4.
- [19] K. Shmelkov, C. Schmid, and K. Alahari, "How good is my gan?," in *Proc. of the Eur. Conf. Comput. Vision (ECCV)*, Sep. 2018.
- [20] A. Borji, "Pros and cons of gan evaluation measures," *Comput. Vision and Image Understanding*, vol. 179, pp. 41–65, 2019.
- [21] Q. Xu *et al.*, "An empirical study on evaluation metrics of generative adversarial networks," *arXiv:1806.07755*, 2018.
- [22] A. Borji, "Pros and cons of gan evaluation measures: New developments," *Comput. Vision and Image Understanding*, vol. 215, 2022.
- [23] W. Pei, B. Xue, L. Shang, and M. Zhang, "A threshold-free classification mechanism in genetic programming for high-dimensional unbalanced classification," in *2020 IEEE Congr. Evol. Comput. (CEC)*, pp. 1–8.
- [24] S. Kotsiantis, D. Kanellopoulos, and P. Pintelas, "Handling imbalanced datasets: A review," *GESTS Int. Trans. on Comput. Sci. and Eng.*, vol. 30, 2006.

- [25] M. Sokolova and G. Lapalme, "A systematic analysis of performance measures for classification tasks," *Inf. Process. & Manage.*, vol. 45, no. 4, pp. 427–437, 2009.
- [26] Z. Zhang, J. Xue, J. Zhang, M. Yang, B. Meng, Y. Tan, and S. Ren, "A deep learning automatic classification method for clogging pervious pavement," *Construction and Building Mater.*, vol. 309, 2021.
- [27] S. Gayathri, V. P. Gopi, and P. Palanisamy, "A lightweight cnn for diabetic retinopathy classification from fundus images," *Biomed. Signal Process. and Control*, vol. 62, 2020.
- [28] R. Sayres *et al.*, "Using a deep learning algorithm and integrated gradients explanation to assist grading for diabetic retinopathy," *Ophthalmology*, vol. 126, no. 4, pp. 552–564, 2019.
- [29] X. Zeng, H. Chen, Y. Luo, and W. Ye, "Automated diabetic retinopathy detection based on binocular siamese-like convolutional neural network," *IEEE Access*, vol. 7, pp. 30744–30753, 2019.
- [30] S. Qummar *et al.*, "A deep learning ensemble approach for diabetic retinopathy detection," *IEEE Access*, vol. 7, pp. 150530–150539, 2019.
- [31] A. Kwasigroch, B. Jarzembinski, and M. Grochowski, "Deep cnn based decision support system for detection and assessing the stage of diabetic retinopathy," in *2018 Int. Interdisciplinary PhD Workshop (IIPhDW)*, pp. 111–116.
- [32] H. Pratt, F. Coenen, D. M. Broadbent, S. P. Harding, and Y. Zheng, "Convolutional neural networks for diabetic retinopathy," *Procedia Comput. Sci.*, vol. 90, pp. 200–205, 2016.
- [33] K. Xu, D. Feng, and H. Mi, "Deep convolutional neural network-based early automated detection of diabetic retinopathy using fundus image," *Molecules*, vol. 22, no. 12, 2017.
- [34] X. Li, T. Pang, B. Xiong, W. Liu, P. Liang, and T. Wang, "Convolutional neural networks based transfer learning for diabetic retinopathy fundus image classification," in *2017 10th Int. Congr. Image and Signal Process., BioMed. Eng. and Inform. (CISP-BMEI)*, pp. 1–11.
- [35] G. Lim, P. Thombre, M. L. Lee, and W. Hsu, "Generative data augmentation for diabetic retinopathy classification," in *2020 IEEE 32nd Int. Conf. Tools with Artif. Intell. (ICTAI)*, pp. 1096–1103.
- [36] M. M. Rahman and D. N. Davis, "Addressing the class imbalance problem in medical datasets," *Int. J. of Mach. Learn. and Comput.*, vol. 3, no. 2, p. 224, 2013.
- [37] D.-C. Li, C.-W. Liu, and S. C. Hu, "A learning method for the class imbalance problem with medical data sets," *Comput. in Biol. and Medicine*, vol. 40, no. 5, pp. 509–518, 2010.
- [38] H. Chen and P. Cao, "Deep learning based data augmentation and classification for limited medical data learning," in *2019 IEEE Int. Conf. Power, Intell. Comput. and Syst. (ICPICS)*, pp. 300–303.
- [39] C. Han *et al.*, "Learning more with less: Conditional pggan-based data augmentation for brain metastases detection using highly-rough annotation on mr images," in *Proc. of the 28th ACM Int. Conf. Inf. and Knowl. Manage., CIKM '19*, p. 119–127, Nov.
- [40] J. Redmon and A. Farhadi, "Yolov3: An incremental improvement," *arXiv:1804.02767*, 2018.
- [41] J. Islam and Y. Zhang, "Gan-based synthetic brain pet image generation," *Brain Inform.*, vol. 7, no. 1, 2020.
- [42] M. Frid-Adar, E. Klang, M. Amitai, J. Goldberger, and H. Greenspan, "Synthetic data augmentation using gan for improved liver lesion classification," in *2018 IEEE 15th Int. Symp. Biomed. Imag. (ISBI)*, pp. 289–293.
- [43] R. Balasubramanian, V. Sowmya, E. A. Gopalakrishnan, V. K. Menon, V. V. Sajith Variyar, and K. P. Soman, "Analysis of adversarial based augmentation for diabetic retinopathy disease grading," in *2020 11th Int. Conf. Comput., Commun. and Netw. Technol. (ICCCNT)*, pp. 1–5.
- [44] C. Han *et al.*, "Combining noise-to-image and image-to-image gans: Brain mr image augmentation for tumor detection," *IEEE Access*, vol. 7, pp. 156966–156977, 2019.
- [45] P. M. Burlina, N. Joshi, K. D. Pacheco, T. A. Liu, and N. M. Bressler, "Assessment of Deep Generative Models for High-Resolution Synthetic Retinal Image Generation of Age-Related Macular Degeneration," *JAMA Ophthalmology*, vol. 137, pp. 258–264, Mar. 2019.
- [46] A. Diaz-Pinto, A. Colomer, V. Naranjo, S. Morales, Y. Xu, and A. F. Frangi, "Retinal image synthesis and semi-supervised learning for glaucoma assessment," *IEEE Trans. on Med. Imag.*, vol. 38, no. 9, pp. 2211–2218, 2019.
- [47] G. HaoQi and K. Ogawara, "Cgan-based synthetic medical image augmentation between retinal fundus images and vessel segmented images," in *2020 5th Int. Conf. Control and Robot. Eng. (ICCCE)*, pp. 218–223.
- [48] D. Hazra and Y.-C. Byun, "Synsiggan: Generative adversarial networks for synthetic biomedical signal generation," *Biol.*, vol. 9, no. 12, 2020.
- [49] K. Joshi, R. Yadav, and S. Allwadh, "Psnr and mse based investigation of lsb," in *2016 Int. Conf. Comput. Techn. in Inf. and Commun. Technol. (ICCTICT)*, pp. 280–285.
- [50] A. Radford, L. Metz, and S. Chintala, "Unsupervised representation learning with deep convolutional generative adversarial networks," *arXiv:1511.06434v2*, 2016.
- [51] "Classification on imbalanced data | TensorFlow Core." tensorflow.org. https://www.tensorflow.org/tutorials/structured_data/imbalanced_data#calculate_class_weights (accessed Feb. 1, 2022).
- [52] "sklearn.ensemble.RandomForestClassifier scikit-learn 1.0.2 documentation." scikit-learn.org. <https://scikit-learn.org/stable/modules/generated/sklearn.ensemble.RandomForestClassifier.html> (accessed Feb. 1, 2022).
- [53] F. Provost and P. Domingos, "Well-trained pets: Improving probability estimation trees," CeDER Working Paper IS-00-04, Stern School of Business, New York University, New York, NY, USA, 2000.